Tear-film breakup: The role of membrane-associated mucin polymers

Anjishnu Choudhury

Department of Mechanical and Aerospace Engineering, Indian Institute of Technology Hyderabad, Telangana 502285, India
and Department of Mathematics, University of British Columbia, Vancouver, British Columbia V6T 1Z2, Canada

Mohar Dey

Department of Mathematics, University of British Columbia, Vancouver, British Columbia V6T 1Z2, Canada

Harish N. Dixit ⓘ

Department of Mechanical and Aerospace Engineering, Indian Institute of Technology Hyderabad, Telangana 502285, India

James J. Feng ⓘ*

Department of Chemical and Biological Engineering, University of British Columbia, Vancouver, British Columbia V6T 1Z3, Canada
and Department of Mathematics, University of British Columbia, Vancouver, British Columbia V6T 1Z2, Canada

Mucin polymers in the tear film protect the corneal surface from pathogens and modulate the tear-film flow characteristics. Recent studies have suggested a relationship between the loss of membrane-associated mucins and premature rupture of the tear film in various eye diseases. This work aims to elucidate the hydrodynamic mechanisms by which loss of membrane-associated mucins causes premature tear-film rupture. We model the bulk of the tear film as a Newtonian fluid in a two-dimensional periodic domain, and the lipid layer at the air-tear interface as insoluble surfactants. Gradual loss of membrane-associated mucins produces growing areas of exposed cornea in direct contact with the tear fluid. We represent the hydrodynamic consequences of this morphological change through two mechanisms: an increased van der Waals attraction due to loss of wettability on the exposed area, and a change of boundary condition from an effective negative slip on the mucin-covered areas to the no-slip condition on exposed cornea. Finite-element computations, with an arbitrary Lagrangian-Eulerian scheme to handle the moving interface, demonstrate a strong effect of the elevated van der Waals attraction on precipitating tear-film breakup. The change in boundary condition on the cornea has a relatively minor role. Using realistic parameters, our heterogeneous mucin model is able to predict quantitatively the shortening of tear-film breakup time observed in diseased eyes.

I. INTRODUCTION

The tear film is essential to the health of the eye as it protects the sensitive epithelium of the cornea and lubricates the eyelid. Only several micrometers thick, it features a complex structure and interesting rheological properties [1]. On the corneal surface is a mucus layer up to half a micrometer in thickness, outside which is an aqueous layer of 2–5 μm that forms the bulk of the tear film. Farthest out is a thin lipid layer that interfaces with the ambient air (Fig. 1). The mucus layer comprises two groups of mucin polymers, membrane-associated mucins (MAMs) attached to the epithelial surface that form a glycocalyx covering the cornea, and gel-forming mucins [2,3]. Each group contains several kinds of mucin molecules. Inside the aqueous layer there is also a small amount of soluble mucins. Altogether the tear film has about 10 mucin species of different molecular weight and properties, produced by different cells and glands in the eye [2,4]. As this work focuses on the MAMs only, for simplicity we will use these three terms interchangeably hereafter: the mucus layer, the MAMs, and the glycocalyx.

The MAMs play an important role in preventing microbial and fungal infections at the ocular surface [6]. Clinical evidence has implicated MAM loss in eye infections and the dry eye syndrome [7,8]. Their highly glycosylated extracellular domains form a tight mesh structure that protects the cornea from pathogenic invasion. In case of a bacterial attack, these extracellular domains get clipped from the epithelial surface and bind with the pathogen to activate an internal signaling pathway for mucosal maintenance and repair [9,10]. Thus, a severe infection can remove MAMs from the epithelial glycocalyx barrier and expose the cornea to the aqueous layer and to direct attack by the pathogens (Fig. 1).

Aside from their role as a physical barrier, recent studies have suggested a second role for MAMs in stabilizing the tear film against premature rupture [3,11]. After each blink, a new tear film is coated over the cornea, which persists in healthy eyes for an extended period before breaking up. This tear-film rupture time t_{rup} falls in a wide range in healthy eyes
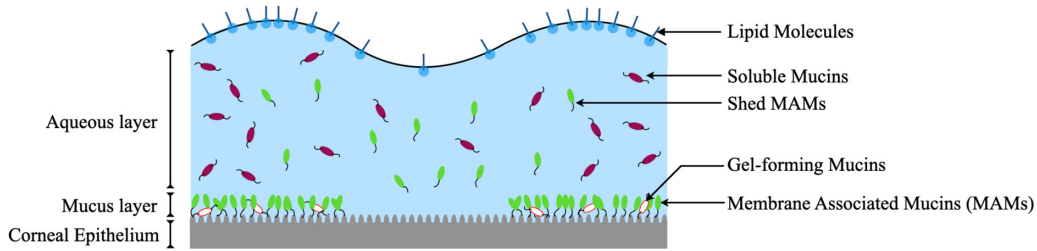
*james.feng@ubc.ca

FIG. 1. Schematic representation of a tear film with a partially damaged mucus layer, with the membrane-associated mucins (MAMs) clipped from the central portion of the corneal epithelium and shed into the aqueous layer. The protrusions on the epithelium represent the corneal microplicae [2,5].

[12], but averages to between 10 and 15 seconds [13,14]. In diseased eyes, however, t_{rup} is shortened to 5 s or less, the most severe cases corresponding to instantaneous breakup [15–17]. The reasons have been hypothesized to be the loss of MAMs [3,11]. A short t_{rup} exposes the cornea to contaminants and pathogens in the ambient air. Thus, the MAMs may protect the cornea through two separate mechanisms, as a physical barrier to pathogens and as a tear-film stabilizer. It is the latter that has inspired the fluid-mechanical study reported here.

How can the loss of MAMs precipitate tear-film breakup? Multiple mechanisms contribute to tear-film breakup, including evaporation [18,19], osmotic flux between the tear film and the cornea [20], nonuniformity in the lipid layer [21,22], gravity-driven drainage [23,24], and van der Waals attraction between the tear-air interface and the corneal surface [12,25–27]. Among these, the van der Waals attraction is most likely to be affected by MAM loss. The other mechanisms produce a rapid initial thinning of the tear film down to about 0.5 μm, after which the van der Waals force dominates and dictates the slower final stage of breakup [12,19,22,28].

Observations suggest that the mucin loss happens in localized regions of the corneal surface, and that the mucin loss amounts to a loss of hydrophilicity. Gipson *et al.* [2,5] presented images showing localized MAM alterations in regions of the corneal epithelium due to keratinization. It is widely accepted that the mucus layer serves to keep the corneal surface hydrophilic [11], and that localized loss of wettability can initiate rapid dewetting and breakup [17,29]. In particular, Gipson *et al.* [5] concluded that "loss of mucins leads to loss of hydration and, in turn, to the formation of dry spots." Winter *et al.* [30] suggested incorporating "varying wettability on the substrate in order to represent unhealthy parts of the cornea." Based on the above, we hypothesize that the loss of MAMs occurs in a spatially heterogeneous manner on the corneal surface, and locally changes its wettability and increases the van der Waals attraction between the interfaces, thus bringing about premature tear-film breakup. To test this hypothesis, we will represent the loss of MAMs by an elevated van der Waals potential in a *heterogeneous mucin model* for tear-film breakup.

We also consider a second mechanism via the change of the boundary condition on the corneal surface. Essentially a polymer meshwork, the glycocalyx should hinder the fluid flow next to the cornea. Such an effect has been demonstrated by calculations of simple shear flows over polymer brushes, where the linear velocity profile in the bulk can be extrapolated toward the substrate to determine an effective negative

slip length [31,32]. With the loss of the MAMs, the exposed cornea surface should take on the usual no-slip boundary condition. The loss of negative slip in the mucin-depleted areas should promote tear-film breakup. Such an effect of the boundary condition may be likened to that of substrate textures on the instability of thin films [33–35].

The objective of this study is to investigate how these two factors affect tear-film breakup. Recently, Dey *et al.* [12] proposed a continuous viscosity model for tear-film breakup by explicitly representing the mucin concentration profile along the depth of the film. An intact glycocalyx was represented by a viscosity profile with a high-viscosity layer atop the cornea, whereas loss of MAMs corresponded to a more or less uniform viscosity profile. This study seeks a more realistic representation of the loss of mucin through an increase in the van der Waals attraction and a change in the boundary condition on the substrate.

II. PROBLEM FORMULATION AND METHODOLOGY

A. Problem description

We pose our problem in a two-dimensional domain that is periodic along the longitudinal x direction, with a homogeneous fluid forming the bulk of the tear film, a lipid layer on top modeled as an insoluble surfactant and a solid substrate with spatially heterogeneous mucin coverage (Fig. 2). Based on descriptions of mucin loss in the literature [5,10], we assume a MAM-depleted area of the cornea between regions with intact MAMs. The fluid above the MAM-depleted area experiences a stronger van der Waals attraction (Hamaker constant $\mathcal{A}_2$) than the rest of the fluid (with $\mathcal{A}_1$). The no-slip condition prevails on the MAM-depleted surface, whereas a negative slip is imposed on the intact MAM. Since the difference between $\mathcal{A}_2$ and $\mathcal{A}_1$ induces a horizontal pressure gradient that drives the flow, we have tested sharp and smooth transitions between the two regions, with the latter represented by a hyperbolic tangent of width δ:

$$\mathcal{A}(x) = \mathcal{A}_1 + \frac{\mathcal{A}_2 - \mathcal{A}_1}{2}\left(\tanh\frac{x - l_1}{\delta} + \tanh\frac{l_1 + l_2 - x}{\delta}\right). \tag{1}$$

The effect of the sharpness of transition turns out to be relatively minor, as will be demonstrated in Sec. III A for a range of δ values. A similar tanh transition is implemented in the slip length β with the same width δ, but its effect is even less and practically negligible. A small sinusoidal initial perturbation is imposed on the interface, and the ensuing breakup process
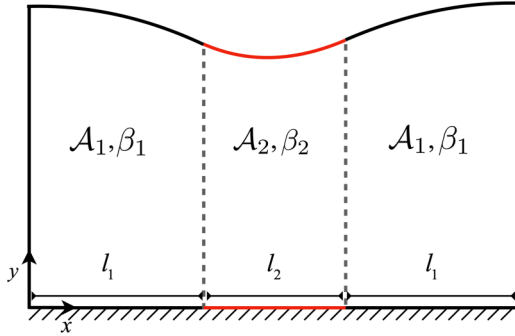
FIG. 2. Schematic of the computational domain. The MAM-depleted region, marked in red on the substrate, has length l_2 and sits in the middle of the domain between two MAM-intact regions of length l_1. The entire domain is periodic along the x direction. The MAM-depleted region features a stronger van der Waals attraction with the interface above it (Hamaker constant $\mathcal{A}_2 > \mathcal{A}_1$) and a no-slip condition on the substrate (Navier slip length $\beta_2 = 0$). The regions with intact MAMs has a negative slip ($\beta_1 < 0$).

is simulated by finite elements until the point of rupture. The basic setup of the problem is similar to that of Dey *et al.* [12], and new features peculiar to this study will be elaborated below.

The tear-film flow is governed by the Navier-Stokes equations:

$$\nabla \cdot \mathbf{u} = 0, \tag{2}$$

$$\rho \left(\frac{\partial \mathbf{u}}{\partial t} + \mathbf{u} \cdot \nabla \mathbf{u} \right) = -\nabla (p + \phi) + \mu \nabla^2 \mathbf{u}, \tag{3}$$

where $\mathbf{u} = (u, v)$ is the velocity vector, p is pressure, and $\phi = -\mathcal{A}/(6\pi h^3)$ is the disjoining pressure due to van der Waals attraction, with $\mathcal{A}$ being the unretarded Hamaker constant and h being the film height. In discussing the results, it will be more intuitive to refer to $-\phi$ as the conjoining pressure as it represents attraction between the interface and the substrate. Following previous models [27,36,37], we use the unretarded van der Waals force instead of the Cassimir or retarded form even though the tear film is relatively thick.

On the air-tear interface, the lipid concentration $\Gamma(x, t)$ is governed by the following surfactant transport equation:

$$\frac{\partial \Gamma}{\partial t} + \nabla_s \cdot (\Gamma \mathbf{u}_s) + \Gamma(\nabla_s \cdot \mathbf{n})(\mathbf{u} \cdot \mathbf{n}) = D_s \nabla_s^2 \Gamma, \tag{4}$$

where $\mathbf{n}$ is the outward normal vector on the surface of the tear film, $\nabla_s = (\mathbf{I} - \mathbf{nn}) \cdot \nabla$ is the surface gradient operator, $\mathbf{u}_s = \mathbf{u} - \mathbf{nn} \cdot \mathbf{u}$ is the tangential velocity vector, and D_s is the surface diffusivity for the insoluble surfactant. Given the complexity in computing the Laplace-Baltrami term accurately (e.g., Ref. [38]), we have adopted the standard treatment in thin-film models of solving the surfactant transport on a straight line and then mapping Γ onto the interface according to the x coordinate [12]. We assume that Γ is dilute and the interfacial tension σ decreases linearly with Γ: $\sigma(\Gamma) = \sigma_m - S\Gamma/\Gamma_m$, where σ_m is the interfacial tension on a lipid-free interface, S is the maximum spreading pressure, and Γ_m is the maximum lipid concentration.

On the interface $y = h(x, t)$ we impose balance of the normal and tangential stresses using the viscous stress tensor $\boldsymbol{\tau}$:

$$\mathbf{n} \cdot \boldsymbol{\tau} \cdot \mathbf{n} = -\sigma(\nabla_s \cdot \mathbf{n}) + p, \tag{5}$$

$$\mathbf{n} \cdot \boldsymbol{\tau} \cdot \mathbf{t} = \nabla_s \sigma \cdot \mathbf{t}. \tag{6}$$

On the solid substrate $y = 0$, we consider the Navier slip boundary condition with a slip length β:

$$u = \beta \frac{\partial u}{\partial y}, \quad v = 0. \tag{7}$$

The slip length $\beta = \beta_2 = 0$ in the portion of the substrate with depleted mucin. In the area covered by intact MAMs, we impose a negative slip length β_1 whose value will be discussed later. The transition is by a tanh profile similar to Eq. (1) with the same width δ.

The setup of the heterogeneous mucin model contains several simplifications. We have neglected evaporation of the tear film [18,19], osmotic flux between the tear film and the cornea [20], rapid rupture due to lipid globs [22], and gravity-driven drainage [23,24]. All can be significant factors in tear-film flow as demonstrated by earlier studies. Braun *et al.* [19] found that most of these factors contribute to a rapid initial thinning the tear film down to about 0.5 μm, at which point van der Waals interaction becomes the dominant factor. Our model essentially starts from this point onward [12]. Another noteworthy factor is the rheology of the tear film. The tear film shows shear-thinning thanks to the many bio-polymers dissolved in it [39,40], and shear-thinning has been included in a few prior models [27,41,42]. Viscoelasticity can also be a factor [43], although an estimation of the mucin relaxation time and concentration in the tear film suggests a negligible elastic stress. Calculations using an Oldroyd-B model indeed show negligible effect of the non-Newtonian rheology. In view of above, and of the focus of the present work on MAM loss, we have excluded the complicating factors from our heterogeneous mucin model.

B. The effective Hamaker constant

There is considerable discrepancy regarding the effective Hamaker constant $\mathcal{A}_1$ for tear film over a healthy cornea with intact MAMs. From the pairwise interfacial energies between the various components (cornea, mucus and water), Sharma *et al.* [25,44] estimated a value of $\mathcal{A}_1 = 10^{-21} \sim 4 \times 10^{-20}$ J, which was used in later studies of tear-film breakup [45]. More recently, Winter *et al.* [30] found that a much larger value $\mathcal{A}_1 = 6.6 \times 10^{-18}$ J was required to reproduce experimental data on the enlargement of dry spots in human tear films. Later, Braun *et al.* [19] used this value to predict tear-film breakup under evaporation and osmotic liquid flux. In their continuous viscosity model, Dey *et al.* [12] used the same value to predict t_{rup} in good agreement with clinical measurements in healthy human eyes. Based on the above, we have decided to adopt $\mathcal{A}_1 = 6.6 \times 10^{-18}$ J in the current model.

We have found no theoretical estimation or experimental measurement of the effective Hamaker constant $\mathcal{A}_2$ for a tear film above a MAM-depleted cornea. Tracing the calculations of Sharma [46] to earlier studies of the apolar Lifshitz-van der
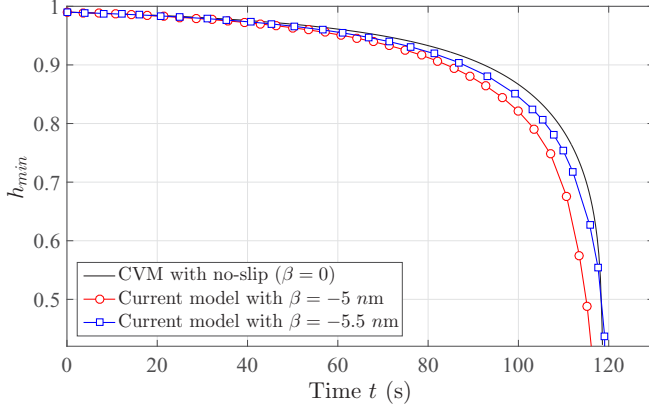
FIG. 3. Determination of the negative slip length β_1 based on matching the tear-film rupture time in a healthy eye. The three curves are the temporal evolution of the minimum film thickness $h_{\min}(t)$ predicted by the continuous viscosity model [12] and the current heterogeneous mucin model for two different values of β_1 over the entire substrate.

Waals interactions between two or more substances [47,48], we can estimate $\mathcal{A}_2$ for a binary cornea–water system from their interfacial tension: $\mathcal{A}_2 = 4.65 \times 10^{-20}$ J. Comparing this with the $\mathcal{A}_1$ values that Sharma [46] estimated using similar arguments, one obtains a ratio $\mathcal{A}_r = \mathcal{A}_2/\mathcal{A}_1$ in the range of $1.16 - 46.5$. Taking this as a rough guideline, we will explore $\mathcal{A}_r$ between 1 and 4 in this study. At $\mathcal{A}_r = 4$, the heterogeneous mucin model already predicts "instantaneous breakup" with a rupture time of a second. Thus, we will not explore $\mathcal{A}_r$ values above 4.

C. Negative slip over mucin-covered cornea

The mucus layer contains the membrane-associated and the gel-forming mucins. Some authors suggested that the gel may act as a lubricant to reduce the viscous friction and produce effective slippage on the cornea [3,49,50]. Given the low viscosity of water, however, we find it difficult to imagine the gel-forming mucins lubricating the tear-film flow. Therefore, we will focus solely on the role of MAMs in hindering fluid flow. This assumption is informed by calculations of shear flow over polymer brushes and networks, which show that the additional resistance due to the polymers amounts to a negative slip; see, e.g., Fig. 4(a) of Ref. [32] and Fig. 2(a) of Ref. [31]. Thus, in the heterogeneous mucin model we have assumed a negative slip length β_1 over intact MAMs. Over the portion of the cornea where MAMs have been shed, we impose the no-slip condition: $\beta_2 = 0$.

The value of β_1 is determined such that our model produces the correct tear-film rupture time t_{rup} for healthy eyes. Dey *et al.* [12] have compiled experimental measurements of t_{rup}, and further developed a continuous viscosity model that successfully predicts the healthy-eye t_{rup}. In their model, the mucus layer is represented by a high-viscosity layer atop the cornea. In our model, β_1 should be such that the negative slip amounts to the same degree of hinderance to tear-film breakup. Figure 3 compares the predictions of the current model and that of Ref. [12]. The current model with $\beta_1 = $

-5.5 nm predicts $t_{\text{rup}} = 119$ s, in good agreement with experimental data and the previous model prediction of $t_{\text{rup}} = 117$ s [12]. This will be used as a baseline value for the rest of the paper.

D. Model parameters

The dimensional parameters involved in the model are summarized in Table I. To facilitate illustration of the highly elongated domain, we adopt two characteristic lengths L and H, and scale the longitudinal lengths by L and the thicknesses by H. Following Braun *et al.* [19], we define the characteristic length L by balancing the viscous and capillary forces. Based on estimations by Ref. [19] using parameters pertinent to human tear films, we take $L = 0.5$ mm. Following Dey *et al.* [12], we choose the length of the computational domain Λ to be the wavelength of the fastest linear mode. In the current model, this choice is complicated by the fact that the heterogeneous mucin loss on the substrate alters the growth rate of the linear instability, and the fastest mode cannot be easily determined *a priori*. To be definite, however, we have chosen Λ corresponding to the homogeneous and intact substrate with full mucin coverage, with $\mathcal{A}_1$ and β_1. The consequences of this choice in tear-film thinning and breakup will be discussed in Sec. III C. Finally, the Hamaker constant $\mathcal{A}_2$ is not listed in the table. We will take $\mathcal{A}_r = \mathcal{A}_2/\mathcal{A}_1 = 2$ as the baseline value, and vary that ratio in the range of 1 to 4.

To make the system of equations and boundary conditions dimensionless, we need two more characteristic quantities besides the length L. We define the characteristic velocity and pressure using the van der Waals driving force:

$$V = \frac{\mathcal{A}_1}{6\pi \mu H L}, \qquad P = \frac{\mathcal{A}_1}{6\pi H^3}. \qquad (8)$$

Consequently, the characteristic time is $T = L/V$. Then nondimensionalization yields the following dimensionless variables (the asterisks will be omitted for brevity in presenting results):

$$x^* = \frac{x}{L}, \quad y^* = \frac{y}{H}, \quad h^* = \frac{h}{H}, \quad u^* = \frac{u}{V}, \quad v^* = \frac{Lv}{HV},$$

$$t^* = \frac{t}{T}, \quad p^* = \frac{p}{P}, \quad \Gamma^* = \frac{\Gamma}{\Gamma_m}, \quad \sigma^* = \frac{\sigma}{\sigma_m},$$

as well as the following dimensionless groups:

Aspect ratio	$\epsilon = H/L,$
Domain length	$\lambda = \Lambda/L,$
Slip lengths	$\bar{\beta}_{1,2} = \beta_{1,2}/H,$
Fraction of MAM-depleted substrate	$f = l_2/\Lambda,$
MAM transition width	$d = \delta/\Lambda,$
Ratio of Hamaker constants	$\mathcal{A}_r = \mathcal{A}_2/\mathcal{A}_1,$
Reynolds number	$\text{Re} = \rho V L/\mu,$
Peclet number	$\text{Pe}_s = V L/D_s,$
Marangoni number	$M = S/\sigma_m,$
Capillary number	$\text{Ca} = \mu V/\sigma_m.$

TABLE I. Parameter values in the model, along with references used for estimating them.

Parameter	Description	Value and source
L	Characteristic length	5×10^{-4} m [19]
H	Initial film thickness	5×10^{-7} m [19]
Λ	Domain length	8.05×10^{-4} m [12]
β_1	Slip length on glycocalyx	-5.5×10^{-9} m (this paper)
β_2	Slip length on exposed cornea	0 (this paper)
δ	Transition layer thickness in Eq. (1)	8.05×10^{-6} m (this paper)
ρ	Density of tear film	1.3×10^{3} kg m^{-3} [51]
μ	Characteristic viscosity of tear film	1.3×10^{-3} Pa s [39]
σ_m	Maximum interfacial tension	4.5×10^{-2} N m^{-1} [52]
S	Maximum spreading pressure	7.5×10^{-8} N m^{-1} [27]
Γ_m	Maximum surfactant concentration	4×10^{-7} mol m^{-2} [53]
$\mathcal{A}_1$	Hamaker constant on glycocalyx	6.6×10^{-18} J [30]
D_s	Surface diffusivity of lipids	3×10^{-8} m^2 s^{-1} [53]

Using the parameter values in Table I, we determine the baseline values of the dimensionless groups: $\epsilon = 10^{-3}$, $\lambda = 1.61$, $\bar{\beta}_1 = -0.011$, $\bar{\beta}_2 = 0$, $f = 1/3$, $\mathcal{A}_r = 2$, Re $= 10^{-6}$, Pe$_s = 0.02$, $M = 1.67 \times 10^{-6}$, and Ca $= 3.11 \times 10^{-8}$. For brevity, we will drop the bar over the dimensionless slip lengths $\bar{\beta}_{1,2}$ in the following. Note that the lengths of the MAM-depleted and MAM-covered regions are constrained by $2l_1 + l_2 = \Lambda$, and we have chosen $f = 1/3$ as the baseline. On the basis of the above, we will vary the parameters $\mathcal{A}_r$, β_1 and f to study the consequences of progressive mucin loss in tear-film breakup. In presenting the results, we will mostly use dimensionless variables. The only exception is the rupture time t_{rup}, for which we also give the dimensional values in certain cases to inform intuition and facilitate comparison with measured values. Note that with the parameter values of Table I, the characteristic time is $T = 357$ s. Initially, the interface is flat at $h_0 = 1$, with a uniform surfactant concentration $\Gamma_0 = 0.5$. The amplitude of the initial sinusoidal perturbation to the interface is $0.01h_0$.

E. Numerics

We perform numerical simulations of the tear-film breakup by solving the Navier-Stokes equations in a two-dimensional domain (Fig. 1) using the finite-element package COMSOL Multiphysics. The moving and deforming interface is tracked by using the arbitrary Lagrangian-Eulerian (ALE) approach with a moving mesh and adaptive mesh refinement. The algorithm refines the mesh near sharp gradients and the moving boundary at every time step. The initial conditions are prescribed as follows:

$$h(x, 0) = 1 + 0.01 \cos\left(\frac{2\pi x}{\lambda}\right), \qquad (9)$$

$$\Gamma(x, 0) = \frac{1}{2} + \Delta\Gamma \cos\left(\frac{2\pi x}{\lambda}\right), \qquad (10)$$

where the perturbation amplitude in the lipid concentration field, $\Delta\Gamma$ is chosen as per linear stability analysis [12,45]. The simulation ends when the tip of the interfacial cusp becomes so pointed that further mesh refinement fails. This typically happens right before the tip reaches the substrate. Thus the

uncertainty in the moment of rupture is small and does not affect the t_{rup} value significantly.

In Dey *et al.* [12], we have already validated several key components of the model, including surfactant transport, Marangoni flows and the conjoining pressure due to van der Waals attraction. The new element in the current implementation is the ALE treatment of interfacial motion. As a validation of the ALE algorithm, we have simulated the Rayleigh-Plateau instability during breakup of a cylindrical filament of a Newtonian fluid, and compared the results with those of Ashgriz and Mashayek [54]. Our results are in very good agreement with the published data, and Fig. 4 presents one such comparison for two solutions obtained at two levels of mesh resolution. Note that our solution hardly changes with mesh refinement. The subsequent solutions are at spatial resolutions equal to or finer than that of the $N = 200$ solution presented here.
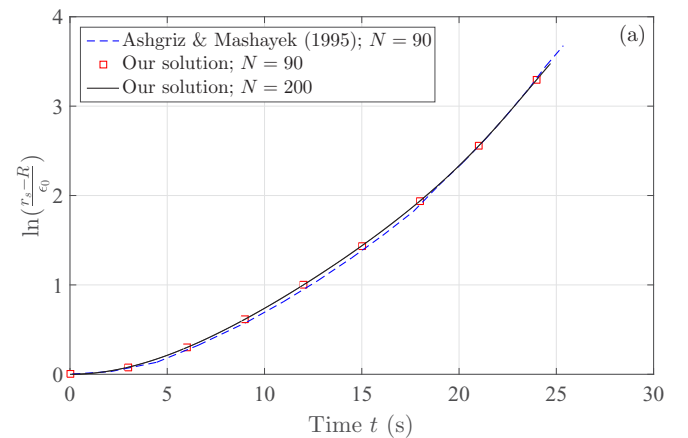

FIG. 4. Validation of our numerical resolution for the capillary breakup of a Newtonian liquid filament against the numerical results of Ashgriz and Mashayek [54] at Re $= 200$ and wavenumber $k = 0.2/R$. R is the mean radius of the filament, r_s is the radius at the crest, ϵ_0 is the initial amplitude of the sinusoidal perturbation, and N is the number of axial elements. Our solutions at the two resolutions practically overlap.
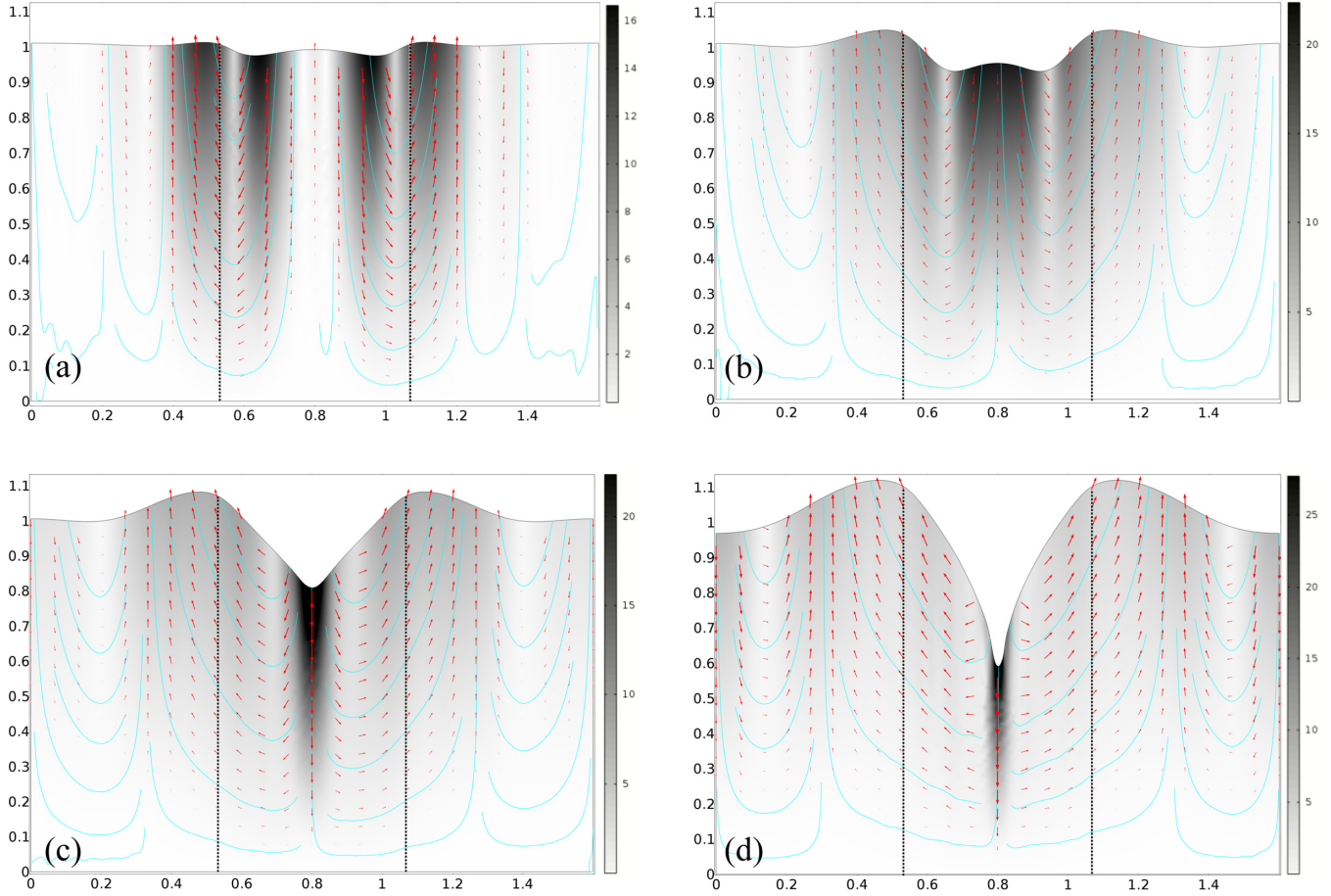
FIG. 5. Tear-film rupture with the central portion of the substrate between the vertical dotted lines being cleared of mucin ($f = 1/3$, $\mathcal{A}_r = 2$, $\beta_1 = -0.011$, $\beta_2 = 0$, $d = 0.01$). The gray scale contours and scale bar show the magnitude of velocity with streamlines superimposed, while the vectors represent velocities with logarithmic magnitude as its length. The frames are at times (a) $t = 0.36$ s, (b) $t = 2.57$ s, (c) $t = 4.65$ s, and (d) $t = 5.21$ s, shortly before the tear-film ruptures at $t = 5.35$ s.

III. RESULTS AND DISCUSSION

In our heterogeneous mucin model, the loss of MAM on the cornea surface is reflected by elevated van der Waals attraction with the tear-air interface, as well as a loss of negative slip on the substrate. In Sec. II C, we have tuned the negative slip β_1 to match the t_{rup} of the healthy tear film. From this starting point, the model predicts progressive shortening of t_{rup} as more of the corneal surface loses mucin coverage. It turns out that the increased van der Waals force is the main cause of the premature tear-film rupture; the loss of negative slip only plays a minor role. We also compare the predictions of the current model with those of the continuous viscosity model [12] and with experimental data for diseased eyes.

A. General characteristics of tear-film rupture

Figure 5 presents the general flow characteristics during tear-film rupture predicted by the heterogeneous mucin model using the baseline parameters of Table I. For this case, the MAM-depleted region occupies a fraction of $f = 1/3$ of the substrate and sits at its center, with a MAM-covered region of equal length on either side. In the initial stage of the simulation, the most salient feature is the appearance of two

interfacial slopes atop the internal boundaries between the MAM-depleted and MAM-covered regions [Fig. 5(a)]. The stronger van der Waals attraction inside drives a flow downward, which then crosses the internal boundaries further down and turns upward just outside the internal boundaries, creating a strongly rotational flow. Because of the large gradient of the conjoining pressure across the internal boundaries, the interfacial distortion is highly localized initially, with a dip inside and a hump outside. This flow creates two local troughs just inside the boundaries that are separated by a peak at the center of the domain. The nature of the van der Waals attraction is such that it drives the dip further down while raises the hump further up, exacerbating the interfacial distortion in time [Fig. 5(b)].

In time, viscous dissipation broadens the flowing regions and moves the two troughs toward each other [Fig. 5(b)]. The downward flow eventually eliminates the central peak and merges the two troughs into a single one [Fig. 5(c)]. Thanks to this change in flow pattern, the central trough is now narrower and well within the two internal boundaries that mark the MAM-depleted portion of the substrate.

From this point onward, the rupture proceeds much as in earlier models with a homogeneous substrate [12,45], with a single trough that is driven further down by the van der
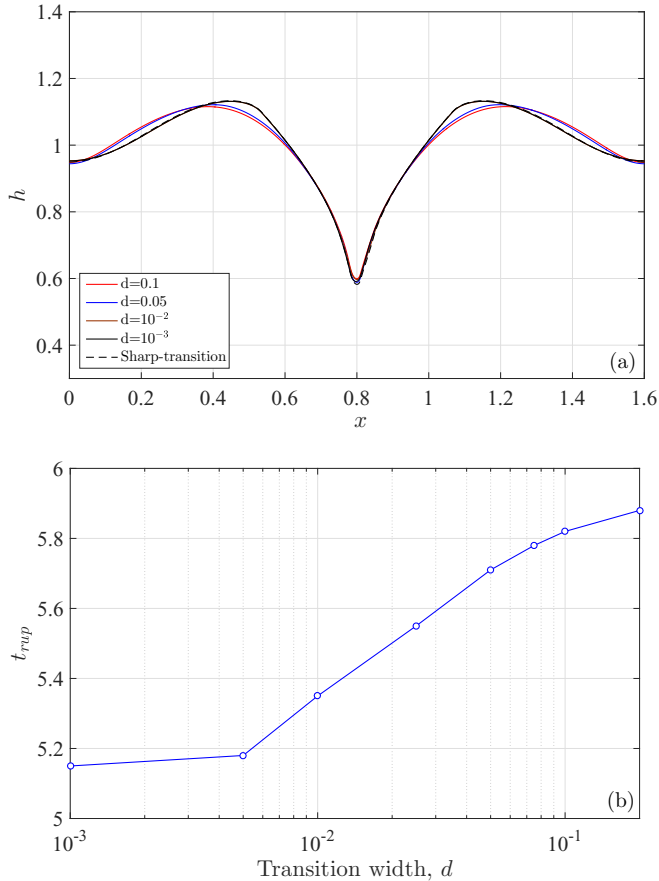
FIG. 6. Effect of the transition width d. (a) The interfacial profile just before breakup. The three profiles for $d = 0$, 10^{-3}, and 10^{-2} practically overlap. (b) The rupture time increases moderately with the transition width.

Waals force against the restoring effects of surface tension and Marangoni stress. Figure 5(d) shows the film profile and velocity contour just before the film ruptures. The negative slip-length β_1 used in the model induces fine vortical structures at the bottom substrate. The wavy streamlines near the bottom in Figs. 5(c) and 5(d) are a manifestation of these fine vortices.

As the film rupture is driven by the gradient of the conjoining pressure across the boundaries between the mucin-intact and mucin-depleted regions, one naturally wonders how the process is affected by the sharpness of the transition [see Eq. (1)]. Figure 6 compares the solutions for several values of the transition width from $d = 0$ (sharp transition) to $d = 0.1$ (more gradual transition). The film profile changes slightly with d, and clearly converges to a "sharp-transition" limit as d falls below 10^{-2} [Fig. 6(a)]. The rupture time $T_{\rm rup}$ increases moderately with d, as may be expected, but exhibits apparent limits at both bounds of the d range tested [Fig. 6(b)]. For lack of experimental data on the transition width, we have chosen $d = 10^{-2}$ (or 8.05 μm), close to the sharp-transition limit, as our baseline value.

B. Effects of the van der Waals force and the no-slip condition

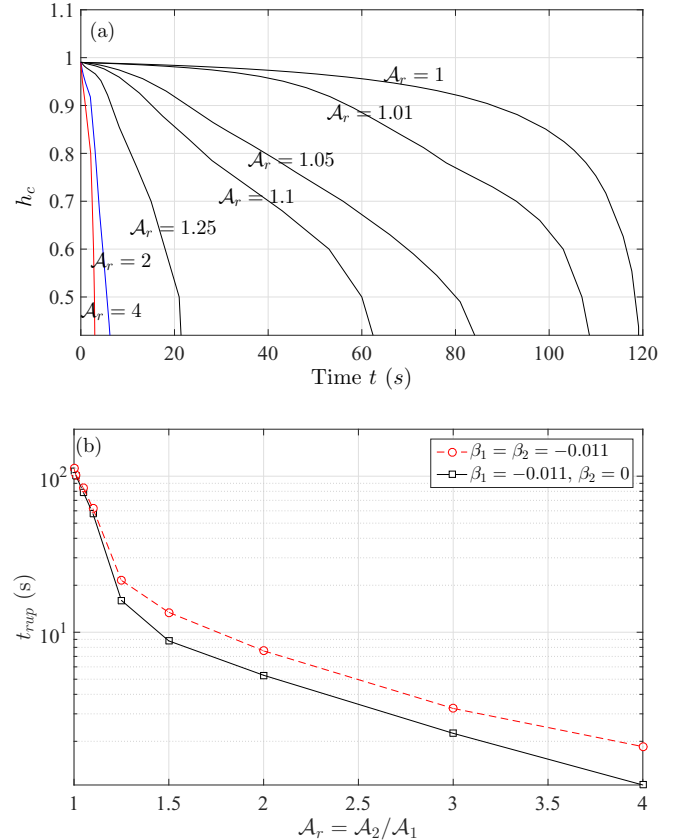We explore separately the effects of an enhanced Hamaker constant and the no-slip condition on breakup of diseased

FIG. 7. Increasing the Hamaker constant $\mathcal{A}_2$ (or equivalently the ratio $\mathcal{A}_r$) hastens tear-film thinning and shortens the breakup time. We have fixed $\mathcal{A}_1$ at the baseline value, $f = 1/3$ and $\beta_1 = \beta_2 = -0.011$. (a) Time evolution of the film thickness h_c at the center of the domain for different values of $\mathcal{A}_r$. (b) The rupture time decreases with increasing $\mathcal{A}_r$. We have also included a curve that corresponds to $\beta_2 = 0$, with no-slip condition on the MAM-depleted region.

tear films. In the first set of simulations, therefore, we vary $\mathcal{A}_2$ while keeping $\beta_2 = \beta_1 = -0.011$, i.e. maintaining the negative-slip boundary condition even in the MAM-depleted area. Besides, we keep the relative size of the MAM-depleted region f and the Hamaker constant $\mathcal{A}_1$ over the intact MAM fixed.

Figure 7 shows the effect of gradually increasing the Hamaker constant $\mathcal{A}_2$ over the MAM-depleted region. The film thins progressively faster with increasing $\mathcal{A}_2$, and the rupture time $t_{\rm rup}$ decreases monotonically [Fig. 7(a)]. This trend is more explicitly shown by the dashed curve of Fig. 7(b). As $\mathcal{A}_r$ increases from 1 to 2, $t_{\rm rup}$ shortens from 119 s to 7.6 s, by a factor of nearly 16. Increasing $\mathcal{A}_r$ to 4 reduces $t_{\rm rup}$ further to 1.9 s. The latter can be considered instantaneous rupture as reported in the experimental literature [15,17]. The decrease of $t_{\rm rup}$ with increasing $\mathcal{A}_r$ is initially very rapid, and then becomes gentler for larger $\mathcal{A}_r$.

A secondary feature is the shape of the thinning curves in Fig. 7(a). With mucin heterogeneity ($\mathcal{A}_r > 1$), the $h_c(t)$ curves change concavity in time. In other words, the thinning speed dh_c/dt is nonmonotonic; it first increases, then decreases before increasing again toward rupture. In contrast, the
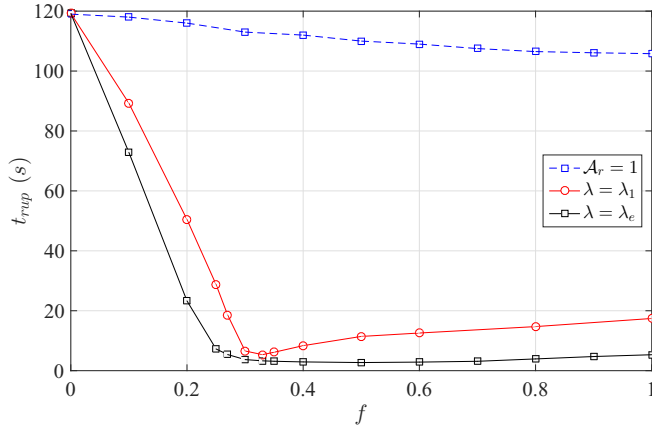
FIG. 8. Effect of expanding the MAM-depleted region on the tear-film rupture time. For the dashed curve, we have imposed the same Hamaker constant on the MAM-depleted region ($\mathcal{A}_r = 1$) but the no-slip boundary condition: $\beta_1 = -0.011$, $\beta_2 = 0$. For the two solid curves, the MAM-depleted region features an elevated van der Waals attraction along with the no-slip boundary condition: $\mathcal{A}_r = 2$, $\beta_2 = 0$. The two curves correspond to different choices of the domain length λ as explained in the text.

homogeneous mucin case ($\mathcal{A}_r = 1$) has a monotonically increasing thinning speed. The temporary slow-down in thinning is probably related to the temporary central hump between the troughs of Fig. 5(b), and is thus a signature of the spatial heterogeneity of the conjoining pressure.

The solid curve in Fig. 7(b) illustrates the effect of changing the boundary condition in the MAM-depleted region from the negative slip ($\beta_2 = \beta_1$) to no slip ($\beta_2 = 0$). This brings about an additional small decrease in the rupture time t_{rup}. Evidently, the loss of negative slip allows faster liquid flow near the substrate, which in turn facilitates the rupture. This effect is more pronounced, in relative terms, for larger values of $\mathcal{A}_r$. But overall it remains much weaker than that of changing $\mathcal{A}_r$. Therefore, between the enhanced van der Waals attraction and the loss of negative slip on the substrate, the former plays the primary role in shortening the breakup time for diseased tear films.

C. Progressive loss of mucin coverage

Clinical evidence points to mucin loss in eye diseases such as bacterial infection and the dry eye syndrome [7,9,10]. In our heterogeneous mucin model, we can represent progressive mucin loss by the expansion of the mucin-depleted area, parametrized by the fraction f. In Sec. III B, we have investigated the roles of an elevated Hamaker constant and loss of negative slip in the MAM-depleted zone at a fixed $f = 1/3$, and come to the conclusion that a higher $\mathcal{A}_2$ markedly shortens the rupture time t_{rup}, while $\beta_2 = 0$ plays only a minor role. Naturally one wonders if this conclusion holds for larger f values, when more of the substrate features the no-slip condition. Figure 8 shows the effect of increasing f. When we only impose the no-slip condition ($\beta_2 = 0$) on the MAM-depleted area without raising the Hamaker constant (dashed curve with $\mathcal{A}_r = 1$), we find a relatively mild decline in the rupture time t_{rup} with increasing f. Compared with the case

of no mucin loss ($f = 0$), loss of the negative slip over a fraction of the substrate ($f = 1/3$) shortens t_{rup} by a mere 5%, and its complete loss over the entire substrate ($f = 1$) causes a reduction of about 11%. This supports the previous conclusion: the loss of negative slip plays a minor role in hastening tear-film rupture even if it prevails over the entirety of the corneal surface.

Now we come to the more realistic case of an expanding MAM-free zone that features both no slip and an elevated $\mathcal{A}_2$. Recall that the domain length λ is fixed at the wavelength λ_1 of the fastest linear mode corresponding to a spatially uniform substrate with Hamaker constant $\mathcal{A}_1$. This protocol has been followed in the simulations presented so far, and the corresponding result is represented by the curve marked $\lambda = \lambda_1$ in Fig. 8. The curve reveals a steep decrease in the rupture time t_{rup} as f increases from 0 to 1/3, at which point t_{rup} has shortened by a factor of 22, from 119 s to 5.4 s. This is consistent with the earlier observations in Fig. 7. Curiously, as f increases further, t_{rup} begins to rise gradually, reaching $t_{\text{rup}} = 17$ s at $f = 1$. This counterintuitive result is mostly due to the fixed domain length $\lambda = \lambda_1$. Without mucin loss ($f = 0$), λ_1 is the wavelength of the fastest linear mode, and nonlinear simulation of breakup in such a domain gives a proper estimation of t_{rup}. With mucin loss and elevated van der Waals attraction, λ_1 may no longer represent the fastest mode. Then the nonlinear simulation will yield an overestimation of t_{rup}.

To test this idea, we have carried out a linear stability analysis by using an analytical result of Zhang *et al.* [45] [Eq. (20) therein], for a homogeneous substrate with $\beta_1 = -0.011$ and other parameters at baseline values. The dispersion relation is depicted in Fig. 9(a) for three values of the Hamaker constant. The tear film becomes progressively unstable with increasing $\mathcal{A}$, and the fastest growing wavenumber increases with $\mathcal{A}$. The corresponding fastest wavelength λ_m declines monotonically with increasing $\mathcal{A}$ [Fig. 9(b)]. This suggests that in our Fig. 8, as $\mathcal{A}$ is raised to $\mathcal{A}_2$ over increasing portions of the substrate, the wavelength of the fastest linear model should become progressively shorter than λ_1. Consequently, the breakup times predicted by the simulations are longer than the true values.

Unfortunately, it is impossible to know *a priori* what the proper wavelength or domain length should be for our heterogeneous substrate with distinct $\mathcal{A}$ values. As a rough estimation, we define an "effective Hamaker constant" $\mathcal{A}_e = (1 - f)\mathcal{A}_1 + f\mathcal{A}_2$, and carry out a series of simulations in which λ is varied according to the fastest wavelength λ_e for a *homogeneous* substrate with $\mathcal{A} = \mathcal{A}_e$. The results are represented by the curve marked by $\lambda = \lambda_e$ in Fig. 8. Note first that the two curves coincide at $f = 0$ as expected. For $f > 0$, the "effectively fastest mode" always outgrows the λ_1 mode, with a shorter t_{rup}. Therefore, it gives a better approximation to the fastest mode that prevails in reality. In particular, the rise of t_{rup} with increasing f beyond $f = 1/3$ has largely disappeared.

The remaining slight increase is attributable to the complexities in the tear-film flow due to heterogeneity of the substrate. These include the rapid rotational flow driven by differing $\mathcal{A}$ across the internal boundaries and the resultant interfacial distortions [Fig. 5(a)], the appearance and
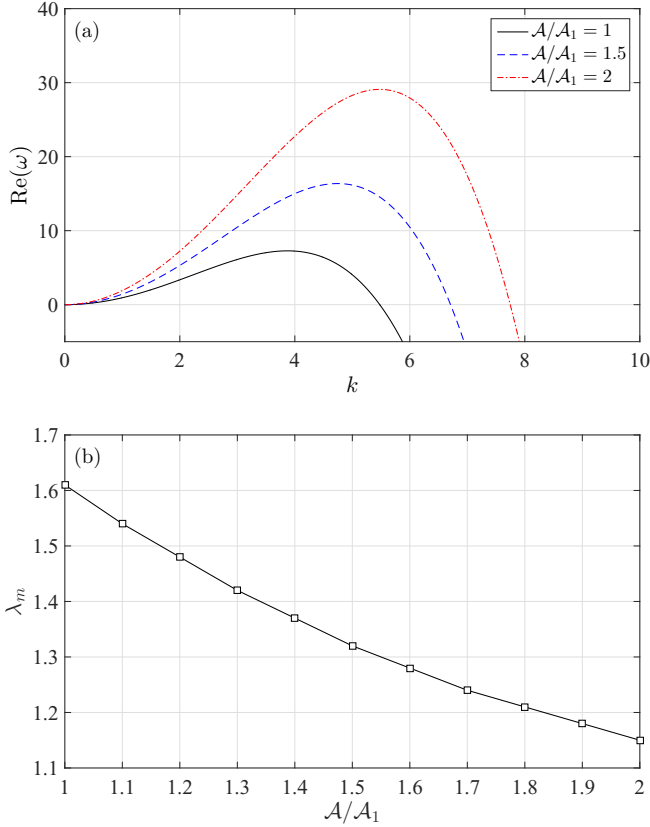
FIG. 9. Linear instability analysis of tear-film breakup on a homogeneous substrate with Hamaker constant $\mathcal{A}$ and slip coefficient $\beta = -0.011$. The other parameters are at baseline values. (a) Dispersion relation for three $\mathcal{A}$ values. (b) The wavelength λ_m decreases monotonically with $\mathcal{A}$.

subsequent merging of the dual valleys [Figs. 5(b) and 5(c)], and the nonmonotonic evolution of the thinning speed in Fig. 7(a). For one, the two internal boundaries are farther apart at larger f values, and the two valleys need to traverse longer distances before merging. This may have contributed to the slight increase in breakup time with increasing f.

D. Comparison with prior studies

It is interesting to compare the predictions of the heterogeneous mucin model with experimental data of shortened t_{rup}, and with prediction of the continuous viscosity model [12]. As the mucin loss extends to about 1/3 of the corneal surface, our model predicts a dramatic shortening of the rupture time from 119 s to 3.3 s (Fig. 8, the $\lambda = \lambda_e$ curve). This prediction is consistent with premature tear-film breakup measured by clinical studies, e.g., 3–4.2 s with eye infections [13] and 5.11 ± 2.74 s for dry-eye patients following infection [14]. With further expansion of the MAM-depleted region, the model predicts essentially a constant rupture time. Note that the model prediction above is based on a doubling of the van der Waals attraction ($\mathcal{A}_r = 2$), which is moderate in view of the range of $\mathcal{A}_r$ estimated theoretically [46].

In the continuous viscosity model [12], a diseased tear film is represented by an abnormally high bulk mucin diffusivity,

such that the viscosity profile relaxes to a uniform one almost instantly, corresponding to rapid diffusion of the MAMs throughout the bulk of the tear film upon being clipped off the corneal surface. In such a limit of rapid diffusion, the film rupture time t_{rup} shortens by a factor of 0.76 according to Fig. 7 of Ref. [12], from 45 s to about 34 s. In contrast, the heterogeneous mucin model predicts a much greater reduction to $t_{\mathrm{rup}} = 3.3$ s if the Hamaker constant $\mathcal{A}_2$ above the MAM-depleted zone is doubled. The latter appears to capture better the premature tear-film rupture observed in experiments [13,14].

Admittedly, at present we cannot ascertain the value of $\mathcal{A}_2$ and the extent of mucin loss in real tear films. The numerical computation is also limited by difficulties in capturing the fastest growing mode of interfacial instability. But the imperfection of the "effectively fastest mode" implies at most a small over-prediction of t_{rup}, and does not affect the main model prediction that mucin loss greatly reduces breakup time of tear films. Taken together, the above comparisons show the advantage of the heterogeneous mucin model over the continuous viscosity model, as well as its potential in explaining the shortening of tear-film rupture time in various eye diseases.

Out of curiosity, we have also explored a "homogeneous mucin loss" model, where we impose an elevated $\mathcal{A}_2$ over the entire domain along with the no-slip boundary condition $\beta_2 = 0$. With increasing $\mathcal{A}_2$, we shorten the domain length λ according to the fastest mode of Fig. 9. Results show that the homogeneous model predicts a longer t_{rup} than the heterogeneous mucin model, and under-predicts the shortening of t_{rup} observed in diseased eyes. For example, the homogeneous model predicts $t_{\mathrm{rup}} = 5.8$ s at $\mathcal{A}_2 = 2$, while the heterogeneous mucin model predicts $t_{\mathrm{rup}} = 3.3$ s with $f = 1/3$ and $\lambda = \lambda_e$ (Fig. 8). This difference may have the same origin as that between $f = 1/3$ and 1 on the $\lambda = \lambda_e$ curve in Fig. 8, and can be attributed to the flow features due to the spatially heterogeneous mucin distribution. The closer agreement between the heterogeneous mucin model and experimental data underscores the observations of localized and nonuniform loss of mucin in diseased eyes [2,5,30].

IV. CONCLUSION

The heterogeneous mucin model reported in this paper is motivated by experimental observations of the loss of membrane-associated mucin polymers (MAMs) in various eye diseases and the concomitant premature breakup of the tear film. It has been hypothesized that the loss of MAMs is the cause for the premature tear-film rupture. We have tested this hypothesis by examining two mechanisms that may contribute to shortening of the tear-film breakup time: an elevated van der Waals attraction over corneal surfaces that have lost its MAMs, and a change of the boundary condition from an effective negative slip on MAM-covered surfaces to no slip on MAM-depleted surfaces. Using finite-element simulations of film rupture, we probed the hydrodynamic consequences of these two factors by assuming a heterogeneous substrate made of MAM-intact and MAM-depleted areas. Within the parameter ranges tested herein, the model predicts the following results:

(a) Both an elevated van der Waals attraction and a loss of negative slip contribute to a shortening of the $t_{\rm rup}$. The former works by strengthening the conjoining pressure that drives the interfacial instability and the latter by facilitating fluid flow near the corneal surface.

(b) The elevated van der Waals force has a much stronger effect; doubling the Hamaker constant over a fraction of the corneal surface can reduce $t_{\rm rup}$ by a factor close to 16. In comparison, loss of negative slip on the same fraction of substrate has a minor effect of a 5% reduction in $t_{\rm rup}$.

(c) The rupture time $t_{\rm rup}$ continues to decrease with progressive expansion of the MAM-free area to about 1/3 of the substrate. The shortened $t_{\rm rup}$ predicted by the model is consistent with clinical data for diseased eyes. With further expansion, the breakup time remains largely unchanged.

(d) The heterogeneous mucin model is superior to the earlier continuous viscosity model as the latter severely underpredicts the shortening in $t_{\rm rup}$ with mucin loss. Thus, a more realistic account of mucin loss on the corneal surface—via changes in wettability and slip condition as opposed to an increase in effective diffusivity—has produced a better model.

The above notwithstanding, we should point out the weaknesses of the current study. The most serious one is perhaps the uncertainty in evaluating the increase in Hamaker constant that accompanies the loss of MAMs. Currently we rely on theoretical estimations of much simplified systems that suggest a rough range of the increase. A direct measurement in the context of the human tear film and cornea will greatly strengthen the basis for our heterogeneous mucin model and allow it to make more quantitative predictions. Second, we have found no experimental data regarding the degree of mucin loss in various eye diseases. In our model, we have represented the progression of mucin loss by the expansion of the mucin-depleted region as a fraction of the entire substrate. This is consistent with the emerging picture in the experimental literature of spatially localized areas of mucin loss or alteration. But no quantification of the loss seems to have been done. Third, the computation is done in a two-dimensional domain that is periodic in the longitudinal direction with a prescribed length λ. This λ corresponds to the wavelength of the most unstable linear mode for a homogeneous corneal surface with a uniform Hamaker constant. As we increase the area of the MAM-depleted region with an elevated Hamaker constant, the fastest linear mode should take on a shorter wavelength. Since this cannot be prescribed *a priori*, our computation cannot faithfully capture the most rapid rupture starting from the appropriate initial perturbation. This is a well-recognized challenge for numerically simulating complex instability problems for which the linear modes are not known. Fourth, the two-dimensionality of the model precludes 3D variations, especially variations in the plane parallel to the corneal surface. Such 3D patterns have been documented by imagining [55] and explored to a limited extent computationally [44,56]. How they affect the tear-film rupture time is an open question. Finally, our model has neglected a host of potentially important factors in tear-film breakup, including non-Newtonian rheology of the tear, evaporation, osmotic flux between the tear film and the cornea, nonuniformity in the lipid layer, and gravity-driven drainage. Such simplifications are perhaps justifiable as we try to focus on the effect of MAM loss on the corneal surface. But to make more quantitative predictions, a more general model should account for such factors with realistic parameters.

ACKNOWLEDGMENTS

[1] R. J. Braun, Dynamics of tear films, Annu. Rev. Fluid Mech. **44**, 267 (2012).

[2] I. K. Gipson, Distribution of mucins at the ocular surface, Exp. Eye Res. **78**, 379 (2004).

[3] B. Yanez-Soto, M. J. Mannis, I. R. Schwab, J. Y. Li, B. C. Leonard, N. L. Abbott, and C. J. Murphy, Interfacial phenomena and the ocular surface, Ocul. Surf. **12**, 178 (2014).

[4] F. Mantelli and P. Argüeso, Functions of ocular surface mucins in health and disease, Curr. Opin. Allergy. Clin. Immunol. **8**, 477 (2008).

[5] I. K. Gipson, Y. Hori, and P. Argüeso, Character of ocular surface mucins and their alteration in dry eye disease, Ocul. Surf. **2**, 131 (2004).

[6] J. P. van Putten and K. Strijbis, Transmembrane mucins: Signaling receptors at the intersection of inflammation and cancer, J. Innate Immun. **9**, 281 (2017).

[7] A.-C. Albertsmeyer, V. Kakkassery, S. Spurr-Michaud, O. Beeks, and I. K. Gipson, Effect of pro-inflammatory mediators on membrane-associated mucins expressed by human ocular surface epithelial cells, Exp. Eye Res. **90**, 441 (2010).

[8] R. M. Corrales, S. Narayanan, I. Fernndez, A. Mayo, D. J. Galarreta, G. Fuentes-Pez, F. J. Chaves, J. M. Herreras, and M. Calonge, Ocular mucin gene expression levels as biomarkers for the diagnosis of dry eye syndrome, Invest. Ophthalmol. Vis. Sci. **52**, 8363 (2011).

[9] T. D. Blalock, S. J. Spurr-Michaud, A. S. Tisdale, and I. K. Gipson, Release of membrane-associated mucins from ocular surface epithelia, Invest. Ophthalmol. Vis. Sci. **49**, 1864 (2008).

[10] C. Wagner, K. Wheeler, and K. Ribbeck, Mucins and their role in shaping the functions of mucus barriers, Annu. Rev. Cell Dev. Biol. **34**, 189 (2018).

[11] A. J. Bron, C. S. de Paiva, S. K. Chauhan, S. Bonini, E. E. Gabison, S. Jain, E. Knop, M. Markoulli, Y. Ogawa, V. Perez, Y. Uchino, N. Yoko, D. Zoukhri, and D. A. Sullivan, TFOS DEWS II pathophysiology report, Ocul. Surf. **15**, 438 (2017).

[12] M. Dey, A. S. Vivek, H. N. Dixit, A. Richhariya, and J. Feng, A model of tear-film breakup with continuous mucin concentration and viscosity profiles, J. Fluid Mech. **858**, 352 (2019); corrigendum **889**, E1 (2020).

[13] Y. Hu, Y. Matsumoto, M. Dogru, N. Okada, A. Igarashi, K. Fukagawa, K. Tsubota, and H. Fujishima, The differences of tear function and ocular surface findings in patients with atopic keratoconjunctivitis and vernal keratoconjunctivitis, Allergy **62**, 917 (2007).

[14] T. Huang, Y. Wang, Z. Liu, T. Wang, and J. Chen, Investigation of tear-film change after recovery from acute conjunctivitis, Cornea **26**, 778 (2007).

[15] N. Yokoi, Y. Takehisa, and S. Kinoshita, Correlation of tear lipid layer interference patterns with the diagnosis and severity of dry eye, Am. J. Ophthalmol. **122**, 818 (1996).

[16] H. Liu, C. G. Begley, R. Chalmers, G. Wilson, S. P. Srinivas, and J. A. Wilkinson, Temporal progression and spatial repeatability of tear breakup, Optom. Vis. Sci. **83**, 723 (2006).

[17] G. A. Georgiev, P. Eftimov, and N. Yokoi, Contribution of mucins toward the physical properties of the tear film: A modern update, Int. J. Mol. Sci. **20**, 6132 (2019).

[18] J. I. Siddique and R. J. Braun, Tear-film dynamics with evaporation, osmolarity and surfactant transport, Appl. Math. Model. **39**, 255 (2015).

[19] R. J. Braun, T. A. Driscoll, C. G. Begley, P. E. King-Smith, and J. I. Siddique, On tear-film breakup (TBU): Dynamics and imaging, Math. Med. Biol. **35**, 145 (2018).

[20] R. J. Braun, N. R. Gewecke, C. G. Begley, P. E. King-Smith, and J. I. Siddique, A model for tear-film thinning with osmolarity and fluorescein, Invest. Ophthalmol. Vis. Sci. **55**, 1133 (2014).

[21] P. E. King-Smith, K. S. Reuter, R. J. Braun, J. J. Nichols, and K. K. Nichols, Tear-film breakup and structure studied by simultaneous video recording of fluorescence and tear-film lipid layer images, Invest. Ophthalmol. Vis. Sci. **54**, 4900 (2013).

[22] L. Zhong, C. F. Ketelaar, R. J. Braun, C. G. Begley, and P. E. King-Smith, Mathematical modelling of glob-driven tear film breakup, Math. Med. Biol. **36**, 55 (2019).

[23] S. Sahlin and E. Chen, Gravity, blink rate, and lacrimal drainage capacity, Am. J. Ophthal. **124**, 758 (1997).

[24] L. Li, R. J. Braun, K. L. Maki, W. D. Henshaw, and P. E. King-Smith, Tear-film dynamics with evaporation, wetting, and time-dependent flux boundary condition on an eye-shaped domain, Phys. Fluids **26**, 052101 (2014).

[25] A. Sharma and E. Ruckenstein, Mechanism of tear-film rupture and formation of dry spots on cornea, J. Colloid Interface Sci. **106**, 12 (1985).

[26] A. De Wit, D. Gallez, and C. I. Christov, Nonlinear evolution equations for thin liquid films with insoluble surfactants, Phys. Fluids **6**, 3256 (1994).

[27] Y. L. Zhang, R. V. Craster, and O. K. Matar, Analysis of tear-film rupture: Effect of non-Newtonian rheology, J. Colloid Interface Sci **262**, 130 (2003).

[28] P. E. King-Smith, C. G. Begley, and R. J. Braun, Mechanisms, imaging, and structure of tear-film breakup, Ocul. Surf. **16**, 4 (2018).

[29] A. Sharma, Breakup and dewetting of the corneal mucus layer, in *Lacrimal Gland, Tear Film, and Dry Eye Syndromes 2*, Advances in Experimental Medicine and Biology, edited by D. A.

Sullivan, D. A. Dartt, and M. A. Meneray, Vol. 438 (Springer, Boston, MA, 1998).

[30] K. N. Winter, D. M. Anderson, and R. J. Braun, A model for wetting and evaporation of a post-blink precorneal tear film, Math. Med. Biol. **27**, 211 (2010).

[31] P. S. Doyle, E. S. G. Shaqfeh, and A. P. Gast, Rheology of polymer brushes: A Brownian dynamics study, Macromolecules **31**, 5474 (1998).

[32] M. Deng, X. Li, H. Liang, B. Caswell, and G. E. Karniadakis, Simulation and modelling of slip flow over surfaces grafted with polymer brushes and glycocalyx fibres, J. Fluid Mech. **711**, 192 (2012).

[33] K. Kargupta and A. Sharma, Templating of Thin Films Induced by Dewetting on Patterned Surfaces, Phys. Rev. Lett. **86**, 4536 (2001).

[34] B. J. Brasjen and A. A. Darhuber, Dry-spot nucleation in thin liquid films on chemically patterned surfaces, Microfluid. Nanofluid. **11**, 703 (2011).

[35] S. Roy, K. J. Ansari, S. S. K. Jampa, P. Vutukuri, and R. Mukherjee, Influence of substrate wettability on the morphology of thin polymer films spin-coated on topographically patterned substrates, ACS Appl. Mater. Interfaces **4**, 1887 (2012).

[36] A. Sharma and E. Ruckenstein, An analytical nonlinear theory of thin film rupture and its application to wetting films, J. Colloid Interface Sci. **113**, 456 (1986).

[37] R. V. Craster and O. K. Matar, Dynamics and stability of thin liquid films, Rev. Mod. Phys. **81**, 1131 (2009).

[38] C. C. de Langavant, A. Guittet, M. Theillard, F. Temprano-Coleto, and F. Gibou, Level-set simulations of soluble surfactant driven flows, J. Comput. Phys. **348**, 271 (2017).

[39] J. M. Tiffany, The viscosity of human tears, Int. Ophthalmol. **15**, 371 (1991).

[40] J. C. Pandit, B. Nagyova, A. J. Bron, and J. M. Tiffany, Physical properties of stimulated and unstimulated tears, Exp. Eye Res. **68**, 247 (1999).

[41] L. Jossic, P. Lefevre, C. de Loubens, A. Magnin, and C. Corre, The fluid mechanics of shear-thinning tear substitutes, J. Non-Newtonian Fluid Mech. **161**, 1 (2009).

[42] R. J. Braun, R. Usha, G. B. McFadden, T. A. Driscoll, L. P. Cook, and P. E. King-Smith, Thin film dynamics on a prolate spheroid with application to the cornea, J. Eng. Math. **73**, 121 (2012).

[43] J. M. Tiffany, Viscoelastic properties of human tears and polymer solutions, in *Lacrimal Gland, Tear Film, and Dry Eye Syndromes*, Advances in Experimental Medicine and Biology, edited by D. A. Sullivan, Vol. 350 (Springer, Boston, MA, 1994).

[44] A. Sharma, R. Khanna, and G. Reiter, A thin film analog of the corneal mucus layer of the tear film: An enigmatic long range non-classical DLVO interaction in the breakup of thin polymer films, Colloids Surf. B **14**, 223 (1999).

[45] Y. L. Zhang, R. V. Craster, and O. K. Matar, Surfactant driven flows overlying a hydrophobic epithelium: Film rupture in the presence of slip, J. Colloid Interface Sci **264**, 160 (2003).

[46] A. Sharma, Acid-base interactions in the cornea–tear film system: Surface chemistry of corneal wetting, cleaning, lubrication, hydration, and defense, J. Dispersion Sci. Technol. **19**, 1031 (1998).

[47] C. van Oss, M. Chaudhury, and R. Good, Monopolar surfaces, Adv. Colloid Interface Sci. **28**, 35 (1987).

[48] C. van Oss, M. Chaudhury, and R. Good, Interfacial Lifshitz–van der Waals and polar interactions in macroscopic systems, Chem. Rev. **88**, 927 (1988).

[49] G. Petrou and T. Crouzier, Mucins as multifunctional building blocks of biomaterials, Biomater. Sci. **6**, 2282 (2018).

[50] Y. Hori, Secreted mucins on the ocular surface, Invest. Ophthalmol. Vis Sci. **59**, DES151 (2018).

[51] Q. Deng, R. J. Braun, and T. A. Driscoll, Heat transfer and tear-film dynamics over multiple blink cycles, Phys. Fluids **26**, 071901 (2014).

[52] B. Nagyova and J. M. Tiffany, Components of tears responsible for surface tension, Curr. Eye Res. **19**, 4 (1999).

[53] M. Bruna and C. J. W. Breward, The influence of non-polar lipids on tear-film dynamics, J. Fluid Mech. **746**, 565 (2014).

[54] N. Ashgriz and F. Mashayek, Temporal analysis of capillary jet breakup, J. Fluid Mech. **291**, 163 (1995).

[55] M. S. Bhamla, C. Chai, N. I. Rabiah, J. M. Frostad, and G. G. Fuller, Instability and breakup of model tear films, Invest. Ophthalmol. Vis. Sci. **57**, 949 (2016).

[56] R. Khanna and A. Sharma, Pattern formation in spontaneous dewetting of thin apolar films, J. Colloid Interface Sci. **195**, 42 (1997).